JACS
JOURNAL OF THE AMERICAN CHEMICAL SOCIETY

ARTICLE

pubs.acs.org/JACS

Synthesis, Photophysical, Electrochemical, and Electrogenerated Chemiluminescence Studies. Multiple Sequential Electron Transfers in BODIPY Monomers, Dimers, Trimers, and Polymer

Alexander B. Nepomnyashchii,[†] Martin Bröring,[‡] Johannes Ahrens,[‡] and Allen J. Bard*[,†]

[†]Center for Electrochemistry, Chemistry and Biochemistry Department, The University of Texas at Austin, Austin, Texas 78712, United States

[‡]Institut für Anorganische und Analytische Chemie, Technische Universität Carolo-Wilhelmina, Hagenring 30, 38106 Braunschweig, Germany

Supporting Information

ABSTRACT: Synthesis of the C^8 BODIPY monomers, dimers, and trimers, a C^8 polymer, and N^8 aza-BODIPY monomer and dimer was carried out. Methyl and mesityl C^8-substituted monomers, dimers, and trimers were used. Dimers, trimers, and polymer were formed chemically through the $\beta-\beta$ (2/6) positions by oxidative coupling using $FeCl_3$. A red shift of the absorbance and fluorescence is observed with addition of monomer units from monomer to polymer for C^8 dyes. The aza-BODIPY dye shows red-shifted absorbance and fluorescence compared with the C^8 analogue. Cyclic voltammetry shows one, two, and three one-electron waves on both reduction and oxidation for the monomer, dimer, and trimer, respectively, for the C^8 BODIPYs. The separation for the reduction peaks for the C^8 dimers is 0.12 V compared with 0.22 V for the oxidation, while the trimers show separations of 0.09 V between reduction peaks and 0.13 V for oxidation peaks. The larger separations between the second and third peaks, 0.25 V for the oxidation and 0.2 V for the reduction, are consistent with a larger energy to remove or add a third electron compared with the second one. The BODIPY polymer shows the presence of many sequential one-electron waves with a small separation. These results provide evidence for significant electronic interactions between different monomer units. The aza-BODIPY dye shows a reduction peak 0.8 V more positive compared to the C^8 compound. Aza-BODIPY dimer shows the appearance of four waves in dichloromethane. The separation between two consecutive waves is around 0.12 V for reduction compared with 0.2 V for oxidation, which is comparable with the results for the C^8 dyes. Electrogenerated chemiluminescence (ECL) of the different species was obtained, including weak ECL of the polymer.

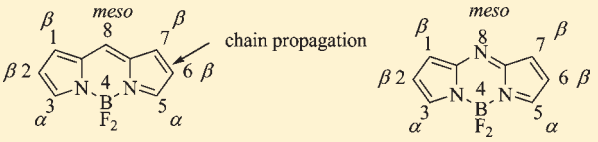

1. INTRODUCTION

BODIPY dyes are of wide importance and have a broad use as laser dyes in biological sensing, electrogenerated chemiluminescence (ECL), and other possible applications.[1−11] Considerable work has also been carried out on their photophysical properties.[1,2,6,7] The absorption and fluorescence properties depend on the position of substitution (see Scheme 1), where addition of a donor substituent to position 8 does not cause a substantial change of the photophysical behavior,[1,12] but bulky donor groups in positions 2 and 6 cause a large red shift in the absorbance and fluorescence.[1] The effect of an acceptor group is different, with a red shift of the absorbance and fluorescence with addition of the acceptor, like a cyano group, to position 8.[1] Addition of a cyano group to positions 2 and 6 causes a smaller change of absorbance and fluorescence wavelength, but it may have a large effect on the fluorescence quantum yield.[1] The presence of bromine atoms in positions 2 and 6 also does not have a substantial effect on the absorbance and fluorescence wavelength.[13] Formation of conjugated systems via positions 2 and 6 also has an effect on the photophysical properties of the BODIPY dyes, showing red-shifted behavior with an increasing degree of conjugation.[14,15] Multiple fluorescence probes for determination of the concentration of metal ions, anions, or neutral molecules can be made by changing the structure of the BODIPY dye. Such probes already have been reported for the determination of Fe^{3+}, Ca^{2+}, Hg^{2+}, Cd^{2+}, CN^-, nitroxyls (HNO), phosphorylated amino acids, and others,[6,7,16−20] including sensitive and selective fluorescent probes.

The electrochemical and ECL properties of these dyes are also of interest.[21−28] BODIPY compounds blocked by alkyl or aromatic groups show one-electron nernstian reduction and oxidation waves for the first electron transfer, where the chemical reversibility depends on the character of substitution.[21,25] The stability of anion radicals depends on substitution in position 8, which is subject to nucleophilic attack, while the cation radicals are stabilized by substitution at the 2 and 6 positions, preventing electrophilic attack.

In this paper we discuss the synthesis of C^8 BODIPY monomers, dimers, trimers, and polymer and aza-BODIPY monomer and dimer (Scheme 2) and investigation of their photophysical, electrochemical, and ECL properties. The monomer, dimer, and trimer of C^8 BODIPY dyes in this study have similar structures, with

Received: February 9, 2011
Published: May 12, 2011

dx.doi.org/10.1021/ja2010219 | J. Am. Chem. Soc. 2011, 133, 8633–8645

either methyl or mesityl groups in the *meso*-position(Scheme 2a−f). The polymer (Scheme 2g) was synthesized with the mesityl substitution to improve its solubility in dichloromethane (DCM) and tetrahydrofuran (THF). Comparative studies of the cyclic voltammetry (CV) of the monomer, dimer, trimer, and polymer can provide information about the electronic interactions among the monomeric units in the reduced and oxidized species,[29−33] as previously studied, for example, with oligothiophenes and oligoanthrylenes.[34−36] Results for the anthracene dimers also show the presence of substantial interaction between different units with separation of about 0.2−0.3 V.[37] Study of the photophysical and structural properties for the anthracene dimers was also carried out to complement the redox data.[38] Electron spin resonance was also shown to be useful for characterization of the oligomers and polymers, as it allows distinguishing between paramagnetic and diamagnetic states, which is very important in conductivity studies.[39,40] The monomer and dimer of aza-BODIPY dyes (Scheme 2h,i), with a nitrogen in position 8 instead of the carbon in C^8 BODIPY, were also studied. These molecules show red or near-infrared fluorescence, as well as less negative reduction, making it easier to study the electrochemistry of the molecules.[41−46] Aza-BODIPY dyes are good candidates for NIR biological probes because of their relatively high quantum yields; few red or NIR probes currently exist.[47,48] pH-responsive fluorescent probes based on N^8 BODIPY have been developed for imaging.[49]

Scheme 1. Structural Representation of the Core of the BODIPY Dyes

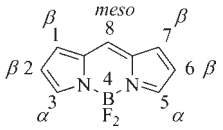

During preparation of this manuscript, we learned that linear dimers and trimers of the BODIPY dyes were synthesized and characterized independently by the Ziessel research group using a different synthetic strategy.[50]

2. EXPERIMENTAL SECTION

2.1. Synthetic Details. *2.1.1. Chemicals and Instrumentation.* All reagents were purchased from Sigma-Aldrich (Germany) and used as received unless stated otherwise. NMR spectra were obtained with Bruker DRX 400 and Bruker Avance 300 spectrometers. Chemical shifts (δ) are given in ppm relative to residual proton solvent resonances (^{1}H, ^{13}C NMR spectra) or to external standards ($BF_3 \cdot Et_2O$ for ^{11}B and $CFCl_3$ for ^{19}F NMR spectra). High-resolution ESI and APCI mass spectra were recorded with a Finnigan LTQ FT. Molecular weight determination by gel permeation chromatography (GPC) relative to a polystyrene standard was carried out in THF through a column of polystyrene sulfonate with a pore size of 5 μm. The pump was a Knauer HPLC 64 with a flow rate of 1 mL min^{-1} and the refractive index detector was a Knauer RI.

2.1.2. Synthesis and Characterization. Compounds **monomer 1**[51] and **aza-BODIPY monomer**[45,52] were prepared according to standard procedures. All other compounds are new, and their synthesis has not been previously published. A schematic of the synthetic procedure is presented in Scheme 3, and the procedures are described below.

Preparation[51] *of* ***monomer 1*** *(1,3,5,7,8-Pentamethyl-4,4-difluoro-4-bora-3a,4a-diaza-s-indacene).* To a solution of 2,4-dimethyl-1*H*-pyrrole (5.4 mL, 52.0 mmol) in dry CH_2Cl_2 (20 mL) is added acetyl chloride (8.7 mL, 121.4 mmol) dropwise at room temperature over 30 min. The deep red solution is heated to reflux for 1 h. The mixture is poured into *n*-hexane (100 mL) after cooling and concentrated to dryness on a rotary evaporator. The resulting dipyrrin hydrochloride is used without any further purification. To a solution of it in dry CH_2Cl_2 (240 mL) is added NEt_3 (20.9 mL, 150 mmol),

Scheme 2. Structural Representation of the BODIPY Monomers, Dimers, and Trimers[a]

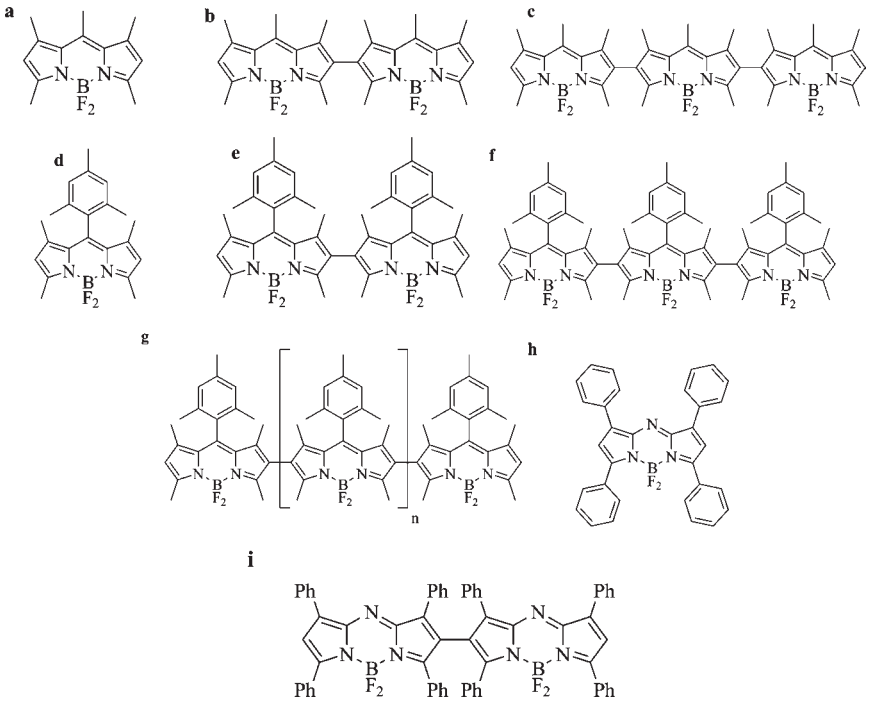

[a] (a,d) **monomer 1** and **monomer 2**; (b, e) **dimer 1** and **dimer 2**; (c, f) **trimer 1** and **trimer 2**; (g) **polymer**; (h) **aza-BODIPY monomer**; and (i) **aza-BODIPY dimer**.

dx.doi.org/10.1021/ja2010219 |*J. Am. Chem. Soc.* 2011, 133, 8633–8645

Scheme 3. Synthetic Procedure for the Compounds Used in the Studies[a]

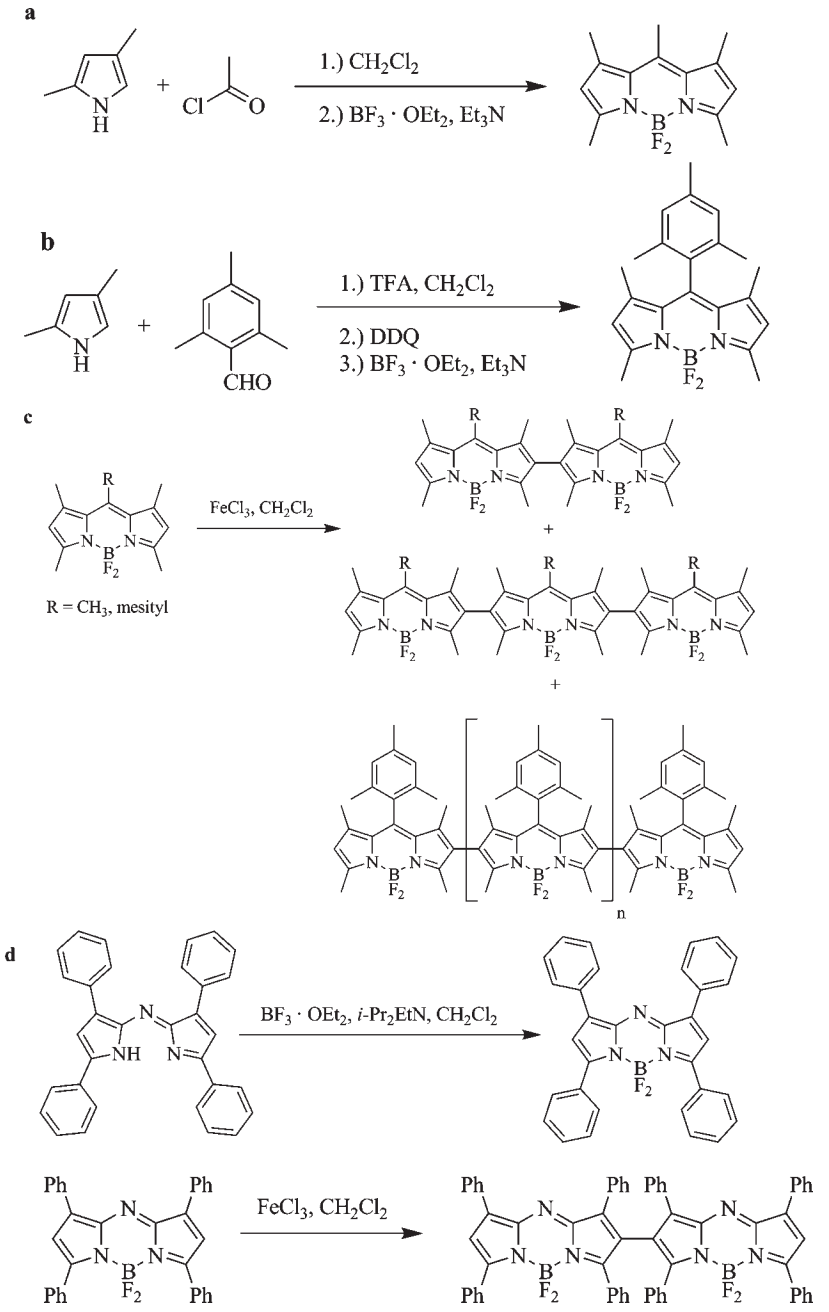

[a] (a) Synthesis of **monomer 1**; (b) synthesis of **monomer 2**; (c) synthesis of C^8 dimers, trimers, and **polymer**; (d) synthesis of **aza-BODIPY monomer**; and (e) synthesis of **aza-BODIPY dimer**.

and the solution is stirred for 10 min at room temperature. $BF_3 \cdot Et_2O$ (27.8 mL, 225 mmol) is added dropwise and stirred for 1 h at room temperature. The deep red solution is washed with saturated aqueous Na_2CO_3 solution (4 × 100 mL), dried over Na_2SO_4, and concentrated on a rotary evaporator. The red, oily residue is purified by column chromatography on silica with *n*-pentane/CH_2Cl_2 = 1:1. The orange-green fluorescing product fraction is dried, and the residue is recrystallized from CH_2Cl_2/MeOH to yield a red-orange, crystalline solid. Yield: 4.924 g, 72%.

^{1}H NMR (400 MHz, $CDCl_3$): δ = 6.05 (s, 2H; 2/6-C*H*), 2.57 (s, 3H; 8-CCH_3), 2.52 (s, 6H; CH_3), 2.41 (s, 6H; CH_3). ^{13}C NMR (100 MHz, $CDCl_3$): δ = 153.8, 141.6, 141.1, 132.2, 121.4 (2C; 2/6-*C*H), 17.4, 16.5, 14.6 (t, J = 2 Hz, 2C; 3/5-CCH_3). ^{19}F NMR (376 MHz, $CDCl_3$): δ = −146.6 (q, J_{BF} = 33 Hz, 2F; BF_2). ^{11}B NMR (128 MHz, $CDCl_3$): δ = 1.30 (t, J_{BF} = 33 Hz, 1B; *B*F_2). HRMS (ESI+): m/z calcd for $C_{14}H_{17}BF_2N_2Na$ $[M+Na]^+$, 285.1345; found, 285.1348.

Preparation of ***dimer 1*** *and* ***trimer 1***. To a solution of 1,3,5,7,8-pentamethyl-4,4-difluoro-4-bora-3*a*,4*a*-diaza-*s*-indacene (**monomer 1**) (195 mg, 0.744 mmol) in dry CH_2Cl_2 (35 mL) is added anhydrous $FeCl_3$ (422 mg, 2.60 mmol) at room temperature. The orange solution rapidly turns deep green-red-violet. The reaction is quenched after 20 min stirring by addition of MeOH (50 mL) and then stirred for an additional 30 min. The organic phase is washed with H_2O (2 × 50 mL), dried over Na_2SO_4, and concentrated to dryness on a rotary evaporator.

dx.doi.org/10.1021/ja2010219 |*J. Am. Chem. Soc.* 2011, 133, 8633–8645

The solid residue is separated by column chromatography on silica with CH_2Cl_2. First the residual educt is eluted as an orange-yellow fraction of greenish yellow fluorescence (100 mg, 51% of recovered educt **monomer 1**). The first product, **dimer 1**, is eluted as an orange fraction of orange-yellow fluorescence followed by the second product, **trimer 1**, as a violet-red fraction of orange fluorescence. Concentrated to dryness, **dimer 1** gives a red solid and **trimer 1** a deep red solid.

Dimer 1 (2,2′-bi-(1,3,5,7,8-pentamethyl-4,4-difluoro-4-bora-3*a*,4*a*-diaza-*s*-indacenyl)): Yield: 55 mg, 27%. ^{1}H NMR (400 MHz, CD_2Cl_2): δ = 6.13 (s, 2H; 6/6′-C*H*), 2.67 (s, 6H; CH_3), 2.51 (s, 6H; CH_3), 2.46 (s, 6H; CH_3), 2.32 (s, 6H; CH_3), 2.23 (s, 6H; CH_3). ^{13}C NMR (100 MHz, CD_2Cl_2): δ = 154.7, 153.4, 142.6, 142.5, 140.1, 133.0, 132.7, 125.2, 122.0 (2C; 6/6′-*C*H), 17.8, 17.3, 15.9, 14.8 (br s, 2C; 5/5′-C*C*H$_3$), 13.5 (br s, 2C; 3/3′-C*C*H$_3$). ^{19}F NMR (376 MHz, CD_2Cl_2): δ = −146.7 (q, J_{BF} = 33 Hz, 4F; 2 × B*F*$_2$). ^{11}B NMR (128 MHz, CD_2Cl_2): δ = 0.37 (t, J_{BF} = 33 Hz, 2B; 2 × *B*F$_2$). HRMS (APCI+): *m*/*z* calcd for $C_{28}H_{33}B_2F_4N_4$ $[M+H]^+$, 523.2822; found, 523.2830.

Trimer 1 (2,2′,6′,2″-tri-(1,3,5,7,8-pentamethyl-4,4-difluoro-4-bora-3*a*,4*a*-diaza-*s*-indacenyl)): Yield: 17 mg, 9%. ^{1}H NMR (400 MHz, CD_2Cl_2): δ = 6.14 (s, 2H; 6/6″-C*H*), 2.75 (s, 3H; 8′-C*C*H$_3$), 2.68 (s, 6H; CH_3), 2.51 (s, 6H; CH_3), 2.47 (s, 6H; CH_3), 2.35 (s, 6H; CH_3), 2.33 (s, 6H; CH_3), 2.26 (s, 6H; CH_3), 2.24 (s, 6H; CH_3). ^{13}C NMR: Due to the low solubility no analyzable ^{13}C NMR spectrum could be recorded. ^{19}F NMR (376 MHz, CD_2Cl_2): δ = −146.6 (m, 6F; 3 × B*F*$_2$). ^{11}B NMR (128 MHz, CD_2Cl_2): δ = 0.59 (t, J_{BF} = 31 Hz, 3B; 3 × *B*F$_2$). HRMS (APCI+): *m*/*z* calcd for $C_{42}H_{48}B_3F_6N_6$ $[M+H]^+$, 783.4118; found, 783.4120.

Preparation of ***monomer 2*** *(8-Mesityl-1,3,5,7-tetramethyl-4,4-difluoro-4-bora-3a,4a-diaza-s-indacene).* To a solution of 2,4,6-trimethylbenzaldehyde (0.73 mL, 5 mmol) and 2,4-dimethyl-1*H*-pyrrole (1.28 mL, 12.5 mmol) in dry CH_2Cl_2 (250 mL) is added a solution of trifluoroacetic acid (50 μL, 0.65 mmol) in dry CH_2Cl_2 (2.5 mL) slowly at room temperature. 2,3-Dichloro-5,6-dicyano-1,4-benzoquinone (1.128 g, 5 mmol) is added after 3 h stirring under ice bath cooling and stirred for 10 min. The solution is stirred for an additional 1 h at room temperature. NEt_3 (10 mL, 72 mmol) is added, followed by slow addition of $BF_3 \cdot Et_2O$ (10 mL, 81 mmol). The reaction mixture is washed after 2 h of stirring at room temperature with saturated aqueous Na_2CO_3 solution (3 × 50 mL), dried over Na_2SO_4, and concentrated on a rotary evaporator. The brown, oily residue is purified by column chromatography on silica with *n*-pentane/CH_2Cl_2 = 5:1, then 2:1, then pure CH_2Cl_2. The product fraction with greenish fluorescence is dried to yield a red-brown solid.

Yield: 1.698 g, 93%. ^{1}H NMR (300 MHz, $CDCl_3$): δ = 6.94 (s, 2H; 2 × mesityl-C*H*), 5.96 (s, 2H; 2/6-C*H*), 2.56 (s, 6H; CH_3), 2.33 (s, 3H; CH_3), 2.10 (s, 6H; CH_3), 1.38 (s, 6H; CH_3). ^{13}C NMR (75 MHz, $CDCl_3$): δ = 155.2, 142.4, 141.8, 138.7, 135.1, 131.3, 130.8, 129.1 (2C; 2 × mesityl-*C*H), 120.9 (2C; 2/6-*C*H), 21.3, 19.6, 14.8 (br s, 2C; 3/5-C*C*H$_3$), 13.5. ^{19}F NMR (376 MHz, $CDCl_3$): δ = −146.5 (q, J_{BF} = 33 Hz, 2F; B*F*$_2$). ^{11}B NMR (128 MHz, $CDCl_3$): δ = 0.69 (t, J_{BF} = 33 Hz, 1B; *B*F$_2$). HRMS (ESI+): *m*/*z* calcd for $C_{22}H_{25}BF_2N_2Na$ $[M+Na]^+$, 389.1971; found, 389.1983.

Preparation of ***dimer 2*** *and* ***trimer 2***. To a solution of 1,3,5,7-tetramethyl-8-mesityl-4,4-difluoro-4-bora-3*a*,4*a*-diaza-*s*-indacene (**monomer 2**) (227 mg, 0.64 mmol) in dry CH_2Cl_2 (30 mL) is added anhydrous $FeCl_3$ (402 mg, 2.48 mmol) at room temperature. The orange solution rapidly turns deep green-red-violet. The reaction is quenched after 25 min stirring by addition of MeOH (25 mL). The organic phase is washed with H_2O (3 × 100 mL), dried over Na_2SO_4, and concentrated to dryness on a rotary evaporator. The solid residue is separated by column chromatography on silica with CH_2Cl_2. First the residual educt is eluted as greenish yellow fluorescing fraction. The first product, **dimer 2**, is eluted as an orange fluorescing fraction, followed by the second product, **trimer 2**, as a reddish fluorescing fraction. Concentrated to dryness, **dimer 2** gives a red solid and **trimer 2** a violet solid.

Dimer 2 (2,2′-bi-(8-mesityl-1,3,5,7-tetramethyl-4,4-difluoro-4-bora-3*a*,4*a*-diaza-*s*-indacenyl)): Yield: 21 mg, 10%. ^{1}H NMR (300 MHz, $CDCl_3$): δ = 6.95 (s, 2H; 2 × mesityl-C*H*), 6.91 (s, 2H; 2 × mesityl-C*H*), 5.97 (s, 2H; 6/6′-C*H*), 2.57 (s, 6H; CH_3), 2.36 (s, 6H; CH_3), 2.32 (s, 6H; CH_3), 2.12 (s, 6H; CH_3), 2.05 (s, 6H; CH_3), 1.39 (s, 6H; CH_3), 1.13 (s, 6H; CH_3). ^{13}C NMR (100 MHz, $CDCl_3$): δ = 155.7, 154.4, 142.8, 141.8, 140.4, 138.8, 135.1, 134.9, 131.4, 131.0, 130.6, 129.3 (2C; 2 × mesityl-*C*H), 129.1 (2C; 2 × mesityl-*C*H), 124.5, 121.2 (2C; 6/6′-*C*H), 21.3, 19.7, 19.7, 14.8 (br s, 2C; 5/5′-C*C*H$_3$), 13.6, 13.5 (br s, 2C; 3/3′-C*C*H$_3$), 12.1. ^{19}F NMR (376 MHz, $CDCl_3$): δ = −146.7 (q, J_{BF} = 33 Hz, 4F; 2 × B*F*$_2$). ^{11}B NMR (128 MHz, $CDCl_3$): δ = 0.57 (t, J_{BF} = 33 Hz, 2B; 2 × *B*F$_2$). HRMS (APCI+): *m*/*z* calcd for $C_{44}H_{49}B_2F_4N_4$ $[M+H]^+$, 731.4085; found, 731.4083.

Trimer 2 (2,2′,6′,2″-tri-(8-mesityl-1,3,5,7-tetramethyl-4,4-difluoro-4-bora-3*a*,4*a*-diaza-*s*-indacenyl)): Yield: 6 mg, 3%. ^{1}H NMR (300 MHz, $CDCl_3$): δ = 6.95 (s, 2H; 2 × mesityl-C*H*), 6.92 (s, 4H; 4 × mesityl-C*H*), 5.98 (s, 2H; 6/6″-C*H*), 2.56 (s, 6H; CH_3), 2.37 (s, 6H; CH_3), 2.34 (s, 6H; CH_3), 2.32 (s, 6H; CH_3), 2.31 (s, 3H; CH_3), 2.12 (s, 6H; CH_3), 2.07 (s, 6H; CH_3), 2.04 (s, 6H; CH_3), 1.39 (s, 6H; CH_3), 1.13 (s, 12H; CH_3). ^{13}C NMR (100 MHz, $CDCl_3$): δ = 155.9, 155.0, 154.3, 142.9, 141.8, 141.7, 140.8, 140.4, 138.9, 138.8, 135.1, 134.9, 134.9, 131.5, 131.4, 131.1, 130.8, 130.6, 129.3 (4C; 4 × mesityl-CH), 129.1 (2C; 2 × mesityl-*C*H), 124.8, 124.4, 121.2 (2C; 6/6″-*C*H), 21.3, 19.8, 19.8, 19.7, 14.8 (br s, 2C; 5/5″-C*C*H$_3$), 13.6, 13.6 (br s) 13.5 (br s), 12.1, 12.1. ^{19}F NMR (376 MHz, $CDCl_3$): δ = −146.8 (m, 6F; 3 × B*F*$_2$). ^{11}B NMR (128 MHz, $CDCl_3$): δ = 0.63 (pseudo t, J_{BF} = 33 Hz, 3B; 3 × *B*F$_2$). HRMS (APCI+): *m*/*z* calcd for $C_{66}H_{72}B_3F_6N_6$ $[M+H]^+$, 1095.6007; found, 1095.6027.

Preparation of ***polymer***. To a solution of 1,3,5,7-tetramethyl-8-mesityl-4,4-difluoro-4-bora-3*a*,4*a*-diaza-*s*-indacene (**monomer 2**) (116 mg, 0.318 mmol) in dry CH_2Cl_2 (30 mL) is added anhydrous $FeCl_3$ (207 mg, 1.27 mmol) at room temperature. H_2O (100 mL) is added to the reaction mixture after stirring for 22 h at room temperature. The separated organic phase is dried over Na_2SO_4 and concentrated to dryness on a rotary evaporator. The blue, solid residue is separated by column chromatography on neutral aluminum oxide (Brockmann activity IV). The smaller units are washed away with CH_2Cl_2. The polymer is finally eluted as a blue fraction with CH_2Cl_2/MeOH = 1:1 and pure MeOH. Phase separation from the coeluted water and filtration leads after evaporation to the product as a violet solid.

Yield: 18 mg. ^{1}H NMR (300 MHz, CD_2Cl_2): δ = 6.94 (br s; mesityl-C*H*), 6.00 (s; C*H*), 3.09−2.80 (br m), 2.56−0.88 (br m). ^{19}F NMR (376 MHz, CD_2Cl_2): δ = −146.6 (m; B*F*$_2$). ^{11}B NMR (128 MHz, CD_2Cl_2): δ = 1.08 (t; *B*F$_2$). GPC (THF, 23 °C, polystyrene standard): M_n = 8732, M_w = 17635, $D(M_w/M_n)$ = 2.02.

Preparation[45,52] *of* ***aza-BODIPY monomer***. To a solution of tetraphenyl azadipyrromethene (414 mg, 0.92 mmol) in dry CH_2Cl_2 (160 mL) is added dry *i*-Pr_2EtN (1.8 mL, 10.1 mmol), and the mixture is stirred for 15 min at room temperature. Freshly destilled $BF_3 \cdot Et_2O$ (1.8 mL, 14.3 mmol) is slowly added and stirred for 24 h at room temperature. The solution is washed with H_2O (3 × 100 mL), dried over Na_2SO_4, and concentrated on a rotary evaporator. The product is dried under vacuum to yield a black-blue solid.

Yield: 468 mg, 100%. ^{1}H NMR (300 MHz, $CDCl_3$): δ = 8.17−7.98 (m, 8H), 7.56−7.35 (m, 12H), 6.99 (s, 2H; 2 × β-C*H*). ^{13}C NMR (100 MHz, $CDCl_3$): δ = 159.7 (2C; aza-BODIPY-*C*), 145.7 (2C; aza-BODIPY-*C*), 144.3 (2C; aza-BODIPY-*C*), 132.4, 131.7, 131.0, 129.7 (t, J = 3 Hz), 129.6, 129.5, 128.8, 128.7, 119.3 (2C; aza-BODIPY-CH). ^{19}F NMR (376 MHz, $CDCl_3$): δ = −133.6 (q, J_{BF} = 31 Hz, 2F; B*F*$_2$). ^{11}B NMR (128 MHz, $CDCl_3$): δ = 0.57 (t, J_{BF} = 31 Hz, 1B; *B*F$_2$). HRMS (APCI+): *m*/*z* calcd for $C_{32}H_{23}BF_2N_3$ $[M+H]^+$, 498.1951; found, 498.1948.

Preparation of ***aza-BODIPY dimer***. To a solution of **aza-BODIPY monomer** (50 mg, 0.100 mmol) in dry CH_2Cl_2 (20 mL) is added anhydrous $FeCl_3$ (65 mg, 0.401 mmol) at room temperature. After stirring

for 30 min, argon-saturated H_2O (40 mL) is added to the reaction mixture and then stirred for an additional 1 h. The blue organic phase is washed with H_2O (2 × 40 mL) and concentrated to dryness on a rotary evaporator. The blue, solid residue is separated by column chromatography on silica with *n*-pentane/CH_2Cl_2= 1:1, then 1:2. First the residual educt is eluted as a blue fraction of red fluorescence, and then the product, **aza-BODIPY dimer**, is eluted as blue fraction. Concentrated to dryness, **aza-BODIPY dimer** is a dark blue powder.

Yield: 21 mg, 43%. ^{1}H NMR (300 MHz, CD_2Cl_2): δ = 8.03−7.90 (m, 8H), 7.54−7.42 (m, 8H), 7.42−7.34 (m, 6H), 7.32−7.03 (m, 20H). ^{13}C NMR: Due to the low solubility no analyzable ^{13}C NMR spectrum could be recorded. ^{19}F NMR (376 MHz, CD_2Cl_2): δ = −130.9 (dq, J_{BF} = 30 Hz, 2F; 2 × BFF), −131.9 (dq, J_{BF} = 30 Hz, 2F; 2 × BFF). ^{11}B NMR (128 MHz, CD_2Cl_2): δ = 0.54 (t, J_{BF} = 30 Hz, 2B, 2 × BF_2). HRMS (APCI+): *m*/*z* calcd for $C_{64}H_{43}B_2F_4N_6$ $[M+H]^+$, 993.3685; found, 993.3666.

2.2. Photophysical and Electrochemical Details. *2.2.1. Chemicals.* Electrochemical grade DCM, ferrocene, and 10-methylphenothiazine were obtained from Aldrich Chemical Co. (Milwaukee, WI) and used without further purification. Supporting electrolytes tetra-*n*-butylammonium hexafluorophosphate ($TBAPF_6$) and benzoyl peroxide were obtained from Fluka.

2.2.2. Apparatus and Methods. UV−vis and fluorescence investigations were carried out in DCM as solvent in air. A DU640 spectrophotometer (Beckman, Fullerton, CA) was used for the absorbance measurements. Fluorescence experiments were carried out under the same conditions using a double-beam QuantaMaster spectrofluorimeter (Photon Technology International, Birmingham, NJ) with a 70 W xenon lamp and slit width of 0.5 mm. Quantum yield calculations were carried out using fluorescein as a standard and compared with known literature results. Electrochemical experiments were done using a three-electrode setup with a 0.0314 cm^2 platinum disk working electrode, platinum wire as a counter electrode, and silver wire as a quasi-reference electrode. The electrode potential was determined using ferrocene as a standard reference material and assuming its potential equal to 0.342 V vs SCE.[53] Larger electrodes with an area of 0.2 cm^2 were used for ECL polymer experiments. A straight platinum electrode was used for all CV measurements, and a bent L-type electrode was used for the ECL investigations. The working electrode was polished for 5 min with 0.3 μm alumina and sonicated for 5 min in EtOH prior to the experiment. The glassware was dried at 120 °C in an oven before transferring to the vacuum chamber of a glovebox (Vacuum Atmospheres Corp., Hawthorne, CA). All solutions for electrochemical measurements were prepared in the glovebox under inert conditions and sealed with a Teflon cap. Three metals rods were drilled through the cap to achieve electrode contact. CV and chronoamperometry pulsing experiments were done using a CH Instruments 660 (Austin, TX) electrochemical workstation. Scan rates 1.0, 0.5, 0.25, and 0.1 V/s were used. Chronoamperometry and scan rate measurements were used to determine the diffusion coefficient values for all species. ECL spectra were generated by stepping the potential to 80 mV past a given peak at a frequency of 10 Hz with 1 min duration. When benzoyl peroxide was used as a co-reactant, stepping was from 0 V to 80 mV after half-wave reduction potential. ECL spectra were recorded with a Princeton Instruments Spec 10 CCD camera (Trenton, NJ) cooled with liquid nitrogen to −100 °C with an Acton SpectPro-150 monochromator. ECL transient measurements were carried out prior to obtaining the ECL spectra. The electrochemical experiments in this case used a multichannel Eco Chemie Autolab PGSTAT100 potentiostat (Utrecht, The Netherlands). The simultaneous ECL-CV signal was recorded with a Hamamatsu (Tokyo, Japan) photomultiplier tube, read with a Keithley electrometer (model 6517, Keithley Instruments, Inc., Cleveland, OH). The relative ECL quantum yield was with reference to $Ru(bpy)_3^{2+}$ under similar conditions. Digital simulations for the CV of monomer, dimer, and trimer were carried out with the Digisim software package (Bioanalytical Systems, West Lafayette, IN).[54−57]

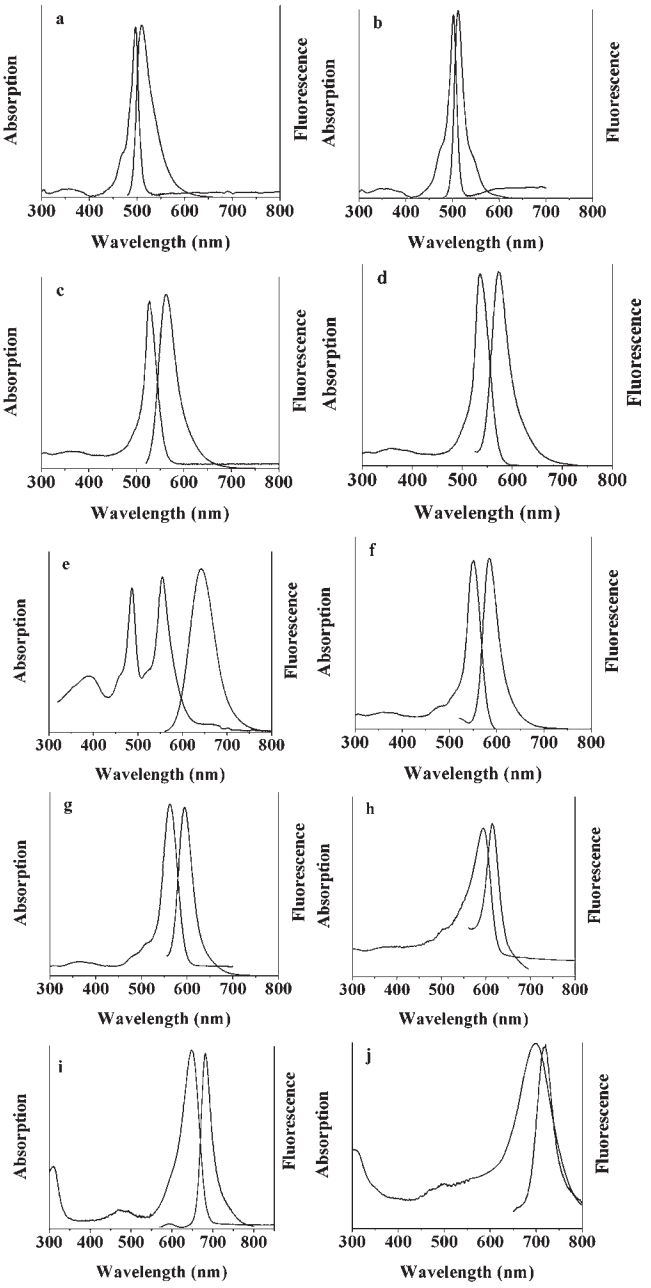

Figure 1. Absorbance and fluorescence spectra of 2 μM BODIPY dyes: (a, b) **monomer 1** and **2**; (c,d) **dimer 1** and **2**; (e) **angular dimer**; (f,g) **trimer 1** and **2**; (h) **polymer**; (i) **aza-BODIPY monomer**; (j) **aza-BODIPY dimer**.

3. RESULTS AND DISCUSSION

3.1. Synthetic Strategy. The synthetic aim of the project was to obtain new oligomeric and polymeric structures of BODIPYs, i.e. dimers, trimers, and small polymers. The best method found is oxidative coupling with anhydrous $FeCl_3$ (~3.5 equiv relative to the BODIPY monomer) in CH_2Cl_2 of double β-free penta-substituted BODIPYs through the 2/6-position. Formation of dimers and trimers (and different higher oligomers) is observed in one pot at room temperature. The reaction is quenched by

Table 1. Photophysical Properties of the Studied BODIPY Compounds

dye	λ_{max} (nm) abs	fluor	ε (10^4 M^{-1} cm^{-1})	Φ_{fluor}	E_s (eV)
monomer 1	353, 497	512	0.75, 8.8	0.97	2.43
monomer 2	359, 501	513	0.74, 8.7	0.97	2.43
dimer 1	368, 526	563	1.5, 15.0	0.66	2.20
dimer 2	368, 535	573	1.6, 15.7	0.66	2.17
trimer 1	370, 550	587	2.3, 22.5	0.60	2.13
trimer 2	372, 562	596	2.35, 23.0	0.60	2.09
polymer	378, 590	614	11.0, 155.0	0.35	2.02
aza-BODIPY monomer	468, 647	682	0.60, 8.5	0.30	1.82
aza-BODIPY dimer	488, 696	720	1.2, 16.0	<0.01	1.72

addition of methanol and/or water after 20−30 min. Although the yields of the dimers (27% and 10%) and trimers (9% and 3%) are low, the unreacted monomers (**monomer 1** and **monomer 2**) can be easily recovered and the oligomers separated by column chromatography. So no additional reaction steps are needed to set up simple monomeric BODIPY for direct coupling. In contrast to this oxidative C−C bond formation via the β-free positions with $FeCl_3$, the reductive coupling and palladium-mediated cross coupling would need an introduction of halogen substituents. [58] The series with the mesityl group at the *meso*-position is much more soluble than the series with the methyl group. Also, short polymers are available if the reaction time is extended to 22 h under otherwise the same conditions. The obtained polymers from **monomer 2** are soluble, and one size of them was even separated by column chromatography to yield **polymer** with a given structure. GPC analysis for this violet compound corresponds to an average of 24 repeating monomer units. To test the versatility of this oxidative coupling over the 2/6-position, the reaction procedure was further extended to **aza-BODIPY monomer**,[52] from which the dimer (**aza-BODIPY dimer**) was obtained in 43% yield despite the steric effect of the phenyl groups.

3.2. Photophysical Results. The photophysical characterization of all the compounds was done in a solution of CH_2Cl_2. **Monomer 1** shows the usual behavior for 2/6-unsubstituted BODIPYs, with a narrow absorption peak at 497 nm and fluorescence with a maximum at 512 nm (Figure 1a). **Monomer 2** shows similar behavior with slightly red-shifted absorbance and fluorescence (Figure 1b). The results are summarized in Table 1. Changing the donor substituent by varying the size of the alkyl or aromatic group in the *meso*-position 8 does not have a significant effect on the fluorescence wavelength. As an example, addition of the bulky amide group, instead of a methyl group, to position 8 causes a shift of the fluorescence of just several nanometers.[59]

The dimers show characteristic S1−S0 and S2−S0 transitions common for the BODIPY dyes (Figure 1c,d). The mesityl-substituted dye also shows slightly red-shifted absorbance and fluorescence compared with the methyl one, similar to monomers. However, there is a huge difference in the behavior of this linear dimer compared with **angular dimer** (Scheme 4).[60,61] The linear dimers show a very small degree of exciton splitting in the absorbance compared with the **angular dimer** with a high degree of splitting and visible presence of the two absorption peaks instead of that seen for the S1−S0 transition (Figure 1e). The **angular dimer** has also red-shifted fluorescence of around 70 to 80 nm compared with the linear dimer.

Scheme 4. Structural Representation of the Angular Dimer

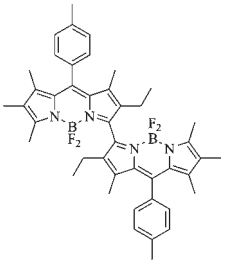

The trimers show behavior similar to the dimers and the absence of the substantial exciton splitting (Figure 1f,g). Comparison of the monomers, dimers, and trimers shows a red shift of the wavelength for the absorbance going from monomer to dimer to trimer, corresponding to the interactions inside a linear alignment of the same chromophors according to the exciton model of Kasha[62] and also partially due to a higher degree of conjugation. Absorbance maxima are red-shifted around 29−34 nm in the case of the transition from monomer to dimer and around 24−27 nm in the case of the transition from dimer to trimer, which shows a smaller change in absorbance properties with addition of consecutive BODIPY units. Fluorescence results show a similar trend, with a large change of around 50 nm in the case of transition from monomer to dimer and only around 20 nm for the transition to trimer. These photophysical properties correspond with an increase of the Stokes shift from 12 to 16 nm for monomers compared with 37 to 38 nm for the dimers and 34 to 37 nm for the trimers. This increase of the Stokes shift corresponds with higher nonradiative decay and a smaller value of the fluorescence quantum yield for the dimer and trimer compared with the monomer. The trimers show a similar Stokes shift to the dimers, probably due to the diminished influence of the interactions with addition of more and more similar units. There is also a smaller change of the quantum yield on going from dimer to trimer relative to the transition from monomer to dimer. The **polymer** shows the appearance of S1−S0 absorbance transition at 590 nm and fluorescence maximum at 614 nm, which is slightly larger than for the trimer, at 596 nm (Figure 1h). The linear **polymer** shows a fluorescence maximum still blue-shifted compared with that of the **angular dimer**.

The **aza-BODIPY monomer** shows red-shifted absorbance and fluorescence compared with the same C^8 dye (Figure 1i), with the characteristic BODIPY dye S2−S0 and S1−S0 transitions. Fluorescence studies show a substantial fluorescence signal for the monomer, although with less efficiency compared with the C^8 dye (Figure 1j). The absorption of the **aza-BODIPY dimer** is red-shifted about 40 nm compared to the monomer. A much higher quenching effect is seen for the dimer, with a quantum yield of less than 0.01.

3.3. Electrochemical Results. Electrochemical studies of the C^8 BODIPY monomers show the presence of one-electron reduction and oxidation waves with separation of around 2.5 V between peaks from first reduction and first oxidation, which is characteristic for green-emitting compounds (Figure 2). All half-wave potentials for the reduction and oxidation and the diffusion coefficients are summarized in Table 2. Electrochemical properties of **monomer 1** were studied previously in acetonitrile and DCM.[21,25] Digital simulations were also carried out to determine the mechanism of the electron transfer (Figures S1 and S2 in the

Supporting Information). Previous studies show a nernstian one-electron transfer for reduction and one-electron oxidation followed by formation of the dimer, with a dimerization constant of 400 M^{-1} s^{-1}.[25] This electrochemical oxidation is consistent with the formation of the dimer chemically using oxidative agent $FeCl_3$ described above. The same mechanism was used in digital simulations for the **monomer 2** (mesityl-substituted dye), which shows similar oxidation and reduction behavior to **monomer 1** (Figure S2 in the Supporting Information). A larger dimerization constant of 2000 M^{-1} s^{-1} was used in simulations.

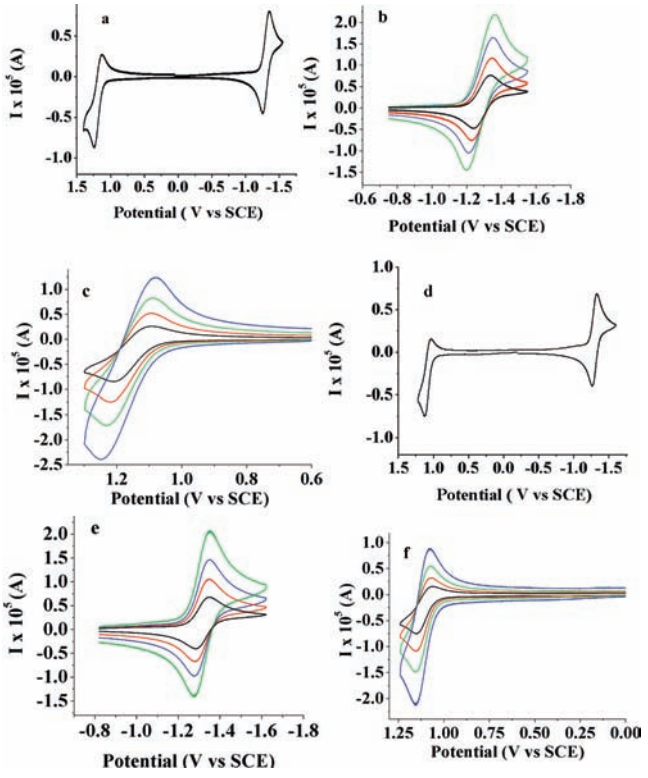

Figure 2. Cyclic voltammograms of (a) 1.1 mM **monomer 1** and (d) 1.0 mM **monomer 2**; (b) and (e) scan rate dependence while scanning in negative and (c) and (f) in positive direction. Solvent, DCM; supporting electrolyte, $TBAPF_6$; platinum electrode area, 0.0314 cm^2.

The mechanism of the dimerization can be represented as

$$R{-}H_2 \rightarrow R{-}H_2^{\cdot+} + e^- \qquad E_{1/2}{}^1 = 1.14\ V \qquad (1)$$

$$R{-}H_2^{\cdot+} + R{-}H_2^{\cdot+} \rightarrow H_2R{-}RH_2^{2+} \qquad k_{dim} = 2000\ M^{-1}\ s^{-1} \qquad (2)$$

$$H_2R{-}RH_2^{2+} \rightarrow HR - RH + 2H^+ \text{ (fast)} \quad k > 10^4 s^{-1} \qquad (3)$$

$$HR{-}RH^{\cdot+} \rightarrow HR{-}RH^{2+} + e^- \qquad E_{1/2}{}^2 = 1.36\ V \qquad (4)$$

$$HR - RH \rightarrow HR{-}RH^{\cdot+} + e^- \qquad E_{1/2}{}^d = 1.10\ V \qquad (5)$$

The mesityl-substituted dye shows a slightly more negative reduction potential compared with the methyl-substituted dye that correlates with a slight red shift of the fluorescence and absorbance.

The dimers show the presence of two one-electron waves on both reduction and oxidation. The fact that the second waves occur as separate ones at more extreme potentials is consistent with a significant interaction between the two BODIPY units (Figure 3a–f). The reduction peak potentials for the **dimer 1** are −1.17 and −1.29 V, compared with the oxidation potentials which are 1.09 and 1.31 V. There is no evidence of substantial dimerization or other chemical processes for both oxidation and reduction products of the dimers, so a simple EE mechanism with two nernstian electrochemical waves was assumed for the simulation (Supporting Information Figures S3 and S4). A small amount of instability on oxidation, however, results in some film formation on repeated cycling, suggesting possible slow coupling, consistent with the absence of substitution in the positions where chain propagation occurs. **Dimer 2** shows similar electrochemical behavior as **dimer 1** with about the same oxidation and reduction potentials. The degree of the separation between reduction

Table 2. Electrochemical Studies of the BODIPY Compounds

	$E_{1/2}$ (V vs SCE)					
dye	A/A^-	A/A^+	λ_{max} (ECL) (nm)	$\Phi_{ECL}{}^a$	ΔH_s (eV)	D (cm^2/s)
monomer 1	−1.21	1.12	545	0.006	2.24	7.0×10^{-6}
monomer 2	−1.19	1.14	538	0.007	2.24	7.0×10^{-6}
dimer 1	−1.17	1.09	587	0.008	2.18	5.2×10^{-6}
	−1.29	1.31				
dimer 2	−1.15	1.10	596	0.008	2.16	5.2×10^{-6}
	−1.27	1.37				
trimer 1	−1.15	1.04	607	0.011	2.09	4.8×10^{-6}
	−1.24	1.17				
	−1.43	1.42				
trimer 2	−1.13	1.11	608	0.016	2.08	4.8×10^{-6}
	−1.23	1.24				
	−1.43	1.50				
polymer	many	many	620	<0.001	1.90	1.4×10^{-6}
aza-BODIPY monomer	−0.44	1.14	695	<0.001	1.40	7.0×10^{-6}
aza-BODIPYdimer	−0.37	1.10	–	–	–	5.2×10^{-6}
	−0.5	1.24				

[a] Relative to $Ru(bpy)_3^{2+}$ under similar conditions.

dx.doi.org/10.1021/ja2010219 |J. Am. Chem. Soc. 2011, 133, 8633–8645

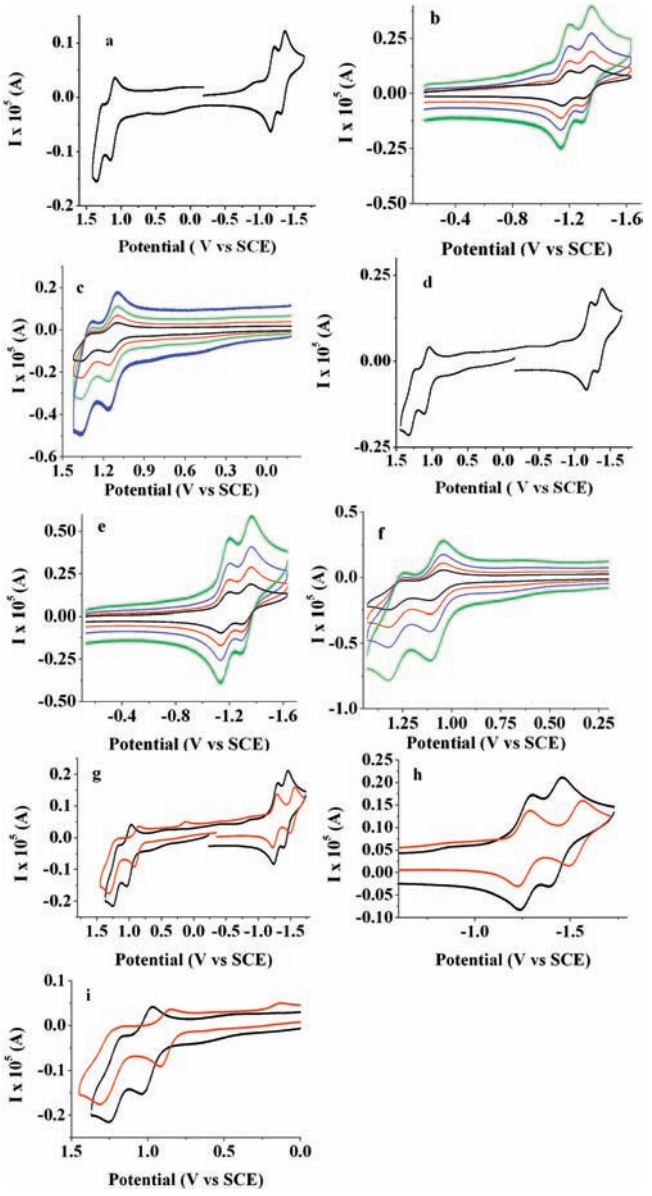

Figure 3. Cyclic voltammograms of (a) 0.14 mM **dimer 1** and (d) 0.3 mM **dimer 2**; scan rate dependence while scanning (b,e) in negative and (c,f) in positive direction; (g−i) comparison of the oxidation and reduction potential between 0.2 mM **dimer 1** and 0.15 **angular dimer**, where in (g) full scan is shown and in (h) and (i) parts for the reduction (h) and oxidation (i) are highlighted. Solvent, DCM; supporting electrolyte, $TBAPF_6$; platinum electrode area, 0.0314 cm^2.

and oxidation waves for both compounds is also substantially less than that of the **angular dimer** (Figure 3g−i), which is electrochemical evidence for a smaller degree of interaction between BODIPY units in case of the dimer formed through position 2/6 compared with position 3. The **angular dimer** also shows the same phenomenon of larger peak separation on oxidation compared with reduction, which seems to be a characteristic feature of these dyes.[28] As a result the larger degree of separation on oxidation cannot be explained by the small instability of the oxidation product as the **angular dimer** has all positions substituted. The reason for the difference in the different amount of separation

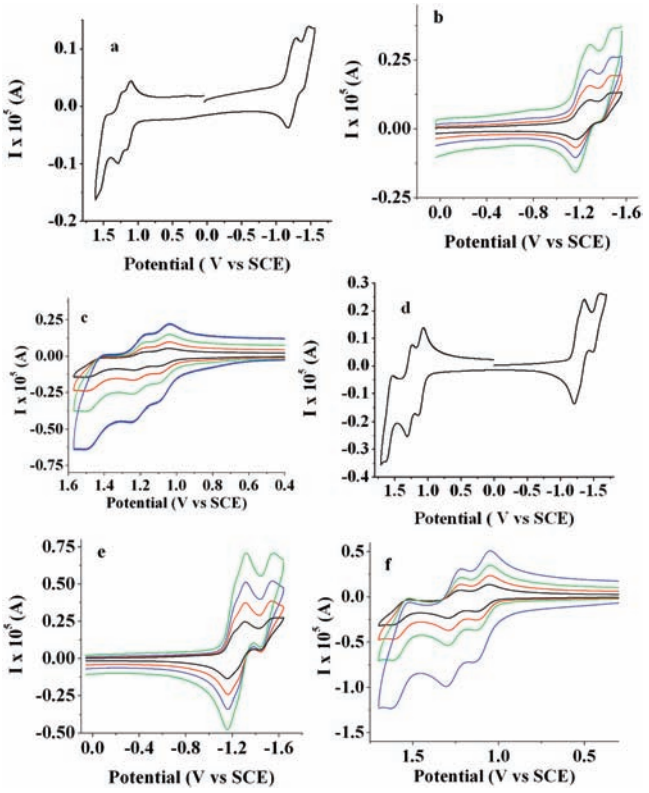

Figure 4. Cyclic voltammograms of (a) 0.1 mM **trimer 1** and (d) 0.24 mM **trimer 2**; scan rate dependence while scanning (b,e) in negative and (c,f) in positive direction. Solvent, DCM; supporting electrolyte, $TBAPF_6$; platinum electrode area, 0.0314 cm^2.

between the two oxidation and the two reduction peaks is not well understood but can probably be related with the extent of delocalization of electron density in charged states and the nature of the electrostatic interactions.[26,63] Work is in progress with oligomers of different monomers to try to resolve this issue.

Trimer 1 shows three one-electron transitions for both oxidation and reduction (Figure 4). The oxidation shows three clear peaks while on reduction the first two peaks are merged to produce a two-electron wave with a shoulder. The reduction half-wave potentials for 0.14 mM of the **trimer 1** are at −1.15, −1.24, and −1.43 V and oxidation half-wave potentials are at 1.04, 1.17, and 1.42 V, as obtained from digital simulations assuming an EE mechanism with three nernstian waves (Supporting Information Figures S5 and S6). **Trimer 2** shows very similar behavior. The trimers show, as the dimers, a smaller separation between the first and second reduction peaks compared with the oxidation. The extent of separation between the two reduction and two oxidation peaks decreases from dimer to trimer. As expected, it is harder to withdraw or add a third electron compared with the second one because of the greater electrostatic repulsion. Similar effects have been seen, e.g., for truxene-oligofluorene compounds[64] and many others. The **polymer** shows the presence of multiple one-electron peaks corresponding to a series of waves, as expected from the results with dimer and trimer (Figure 5). This is especially clear for the experiment in THF, where appearance of about 20 consecutive reduction waves is noticed. A diffusion coefficient of 1.4×10^{-6} cm^2/s was estimated by using eq 6[29]

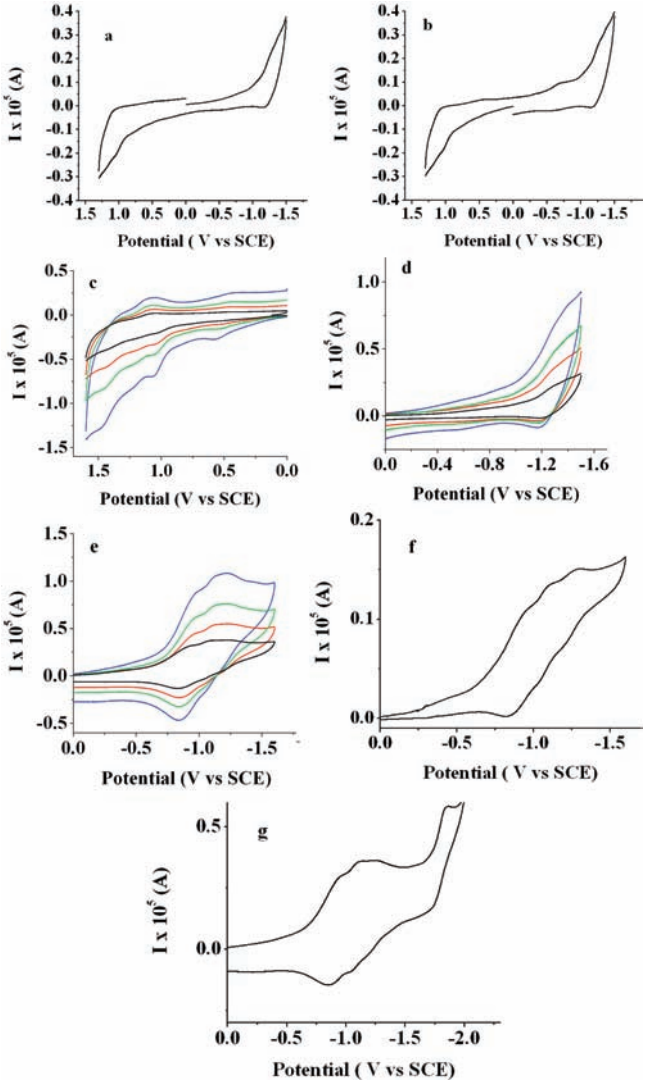

Figure 5. Cyclic voltammograms of 0.15 mM **polymer** in DCM during scan in (a) negative and (b) positive direction; scan rate dependence during scan in (c) negative and (d) positive direction, for 1 (blue), 0.5 (green), 0.25 (red), and 0.1 V/s (black). (e–g) Cyclic voltammograms of **polymer** in THF: (e) scan rate dependence for 0.15 mM **polymer**, for 1 (blue), 0.5 (green), 0.25 (red), and 0.1 V/s (black); (f) scan rate 0.01 V/s; (g) scan to −2.5 V. Electrode area, 0.0314 cm^2; supporting electrolyte, $TBAPF_6$.

from the overall limiting current values.

$$(D_p/D_m) = (M_m/M_p)^{0.55} \quad (6)$$

It is difficult to simulate the **polymer** CV behavior because of the polydispersity of the polymer and also the influence of many peak splittings and rate constants on the electrochemical reduction process. This can also cause a deviation of the number of electron transfers from the number expected from the gel permeation studies, 24, and the expected diffusion current. The oxidation also shows multiple electron transfers, but observation of all multiple transitions is limited by the potential window.

The **aza-BODIPY monomer** shows a nernstian reduction wave with a peak potential shifted positive by about 0.8 V compared to the C^8 BODIPY (Figure 6). It is possible to see a second

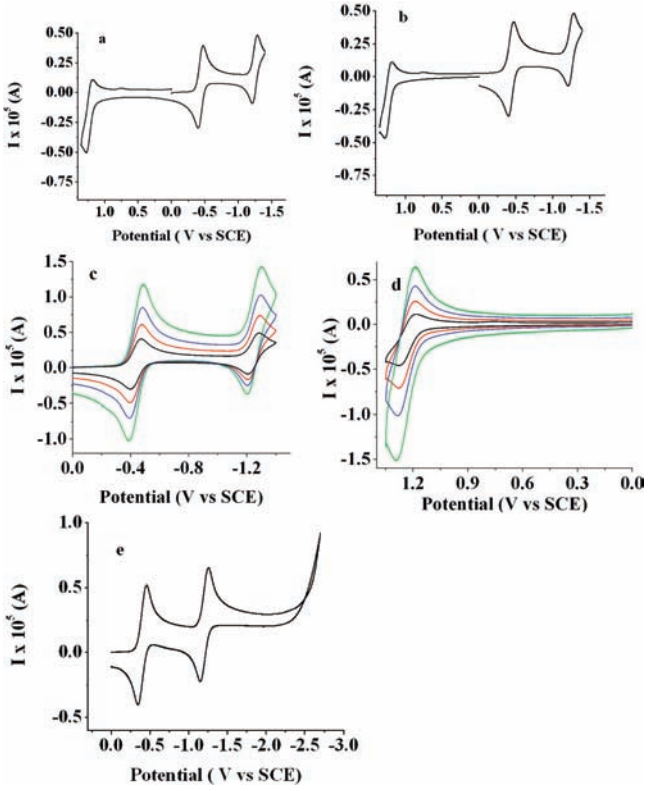

Figure 6. Cyclic voltammograms of 0.6 mM **aza-BODIPY monomer** at a scan rate of 0.1 V/s in DCM at platinum working electrode. Area, 0.0314 cm^2; supporting electrolyte, 0.1 M $TBAPF_6$. (a) Forward scan to the negative direction; (b) forward scan to the positive direction; scan rate dependence for oxidation (c) and reduction (d); (e) scan for 0.8 mM **aza-BODIPY monomer** in THF.

reversible reduction wave for this species in DCM (Figure 6a–c,e). The separation between the two reduction waves is around 0.82 V, which is smaller than 1.09 V seen for the C^8 system (which shows unusually large separations between the first two electron additions).[25] The separation between consecutive peaks is, however, still larger than that in 9,10-diphenylanthracene and other polycyclic hydrocarbons (about 0.5 V).[65–67] A slight decrease in the separation between the two reduction waves is seen with addition of the acceptor group, i.e., 1.09 V for alkyl-substituted dye and 0.98 V for the 8-cyano-substituted dye,[25] compared to that with the acceptor atom nitrogen, i.e., 0.82 V for aza-BODIPY. Reduction of the **aza-BODIPY monomer** in THF at more negative potentials shows the absence of any electrochemical processes up to −3.0 V (Figure 6e). Digital simulation confirmed the reversibility of the second electron reduction (Supporting Information Figure S7a–d). As with the C^8 BODIPY, oxidation of the aza-compound also shows some dimer formation. Simulations including formation of the dimer on oxidation were carried out and show a rate of dimerization about the same as with the analogous C^8 BODIPY (Supporting Information Figure S7e–h). The **aza-BODIPY dimer** shows four reduction waves in DCM. The first two transitions correspond to the addition of one electron to each monomer unit and the second one to the addition of an additional electron to each unit (Figure 7). An experiment with the analogous C^8 **dimer 2** in THF at room temperature also shows the presence of four peaks at more negative potentials, but the reversibility is much poorer under these conditions (Figure 7e).

dx.doi.org/10.1021/ja2010219 |*J. Am. Chem. Soc.* 2011, 133, 8633–8645

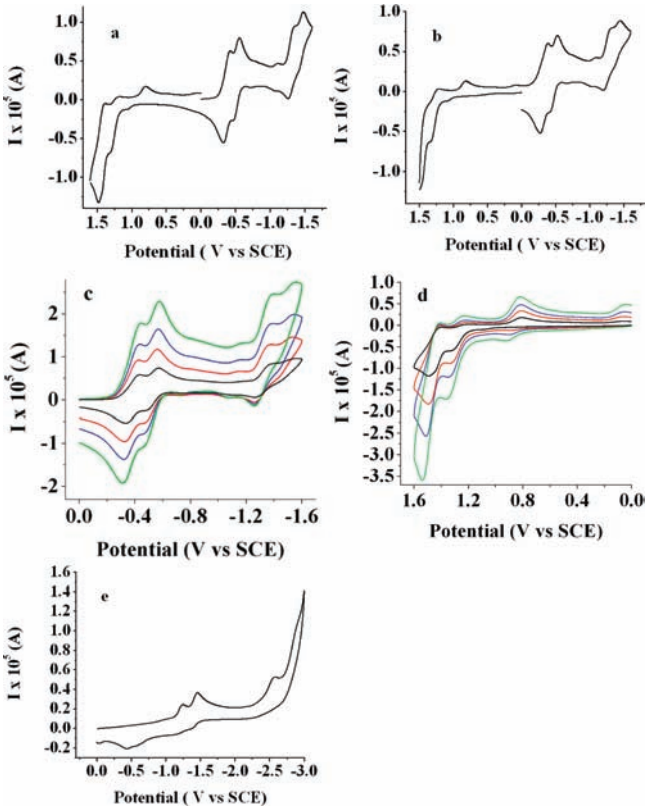

Figure 7. Cyclic voltammograms of 0.9 mM **aza-BODIPY dimer** at a scan rate of 0.1 V/s in DCM at platinum working electrode. Area, 0.0314 cm^2; supporting electrolyte, 0.1 M $TBAPF_6$. (a) forward scan to the negative direction; (b) forward scan to the positive direction; scan rate dependence for (c) oxidation and (d) reduction; (e) reduction of 0.3 mM of **dimer 2** in THF.

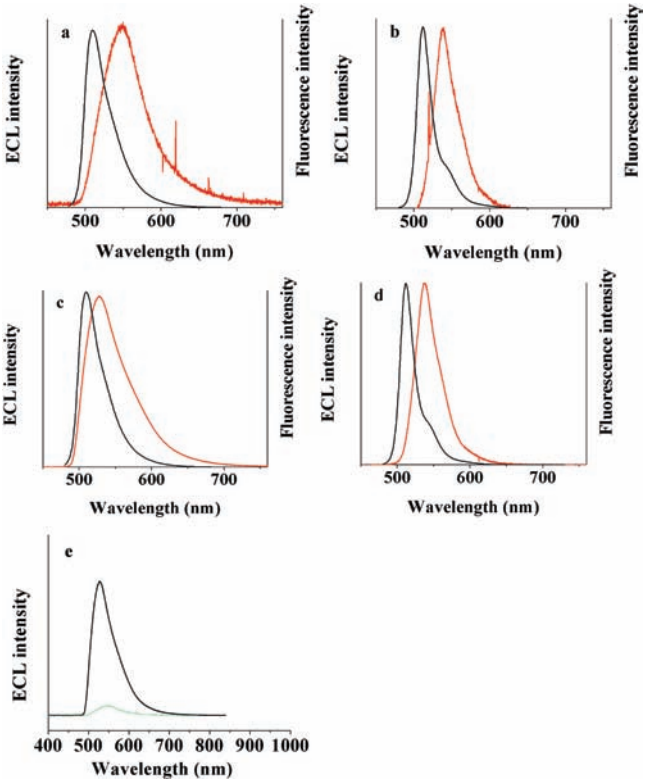

Figure 8. Electrogenerated (red line) and fluorescence (black line) of investigated monomers. Annihilation spectrum for (a) 1.0 mM **monomer 1** and (b) 1.1 mM **monomer 2**. (c,d) Spectra generated in the presence of 5 mM of benzoyl peroxide. (e) Comparative spectra of the annihilation results (green) and in the presence of co-reactant (black). Solvent, DCM; supporting electrolyte, 0.1 M $TBAPF_6$; platinum electrode area, 0.0314 cm^2.

Digital simulations can be fit to the experimental results with some deviation for waves 3 and 4, probably because of kinetic complications and instability of the 3- and 4-species (Supporting Information Figure S8). The separation between the first two sequential waves (and also the third and fourth wave) was ~0.12 V, very close to the results for the C[8] BODIPY dimers. The separation between the first two waves on oxidation is larger than that for the reduction. The separation between the first and third reduction wave was ~1.0 V, which is similar to the results for the monomer. The reason for that was determined to be steric in the aza-BODIPY core.[25]

3.4. ECL Results. ECL of both the monomers showed relatively weak emission while stepping in both positive and negative directions (Figure 8).[21,25] However, the intensity was sufficient to be able to obtain ECL spectra (Figure 8a,b). The annihilation ECL mechanism can be represented as

$$\mathrm{BODIPY} + e^- \rightarrow \mathrm{BODIPY}^{\cdot -} \quad (7)$$

$$\mathrm{BODIPY} - e^- \rightarrow \mathrm{BODIPY}^{\cdot -}\ (\mathrm{unstable}) \quad (8)$$

$$\mathrm{BODIPY}^{\cdot -} + \mathrm{BODIPY}^{\cdot -} \rightarrow \mathrm{BODIPY}^* \quad (9)$$

$$\mathrm{BODIPY}^* \rightarrow \mathrm{BODIPY} + h\nu \quad (10)$$

The low intensity of the ECL is related to absence of the substitution in positions 2 and 6, causing instability of the radical cation. The ECL efficiency could be enhanced by using oxidative correactant benzoyl peroxide (BPO), which allows light generation without electrochemical oxidation of the dye:[68−70]

$$\mathrm{BODIPY} + e^- \rightarrow \mathrm{BODIPY}^{\cdot -} \quad (11)$$

$$\mathrm{BODIPY}^{\cdot -} + \mathrm{BPO} \rightarrow \mathrm{BODIPY} + \mathrm{BPO}^{\cdot -} \quad (12)$$

$$\mathrm{BPO}^{\cdot -} \rightarrow \mathrm{C_6H_5CO_2}^- + \mathrm{C_6H_5CO_2}^{\cdot} \quad (13)$$

$$\mathrm{BODIPY}^{\cdot -} + \mathrm{C_6H_5CO_2}^{\cdot} \rightarrow \mathrm{BODIPY}^* + \mathrm{C_6H_5CO_2}^- \quad (14)$$

The ECL emission was about 15 times larger with the co-reactant and also showed a much higher stability with time compared with the annihilation ECL (Figure 8e). The ECL annihilation spectrum can be generated only for a few minutes, while in the presence of the benzoyl peroxide it was stable for more than an hour. The ECL spectral maximum was similar to that of the fluorescence with the slight difference due to an inner filter effect. No features that can be assigned to formation of the dimer, trimer or some other species were seen. The same relatively weak annihilation intensity was found with the dimers and trimers (Figures 9 and 10), with dimers showing perhaps a bit higher ECL annihilation emission, and trimers slightly higher compared with the monomer (Figures 9a,b and 10a,b). There is also an increase in ECL intensity with the addition of the benzoyl peroxide for both dimers and trimers (Figures 9c,d and 10c,d).[21] The ECL maxima

dx.doi.org/10.1021/ja2010219 |J. Am. Chem. Soc. 2011, 133, 8633–8645

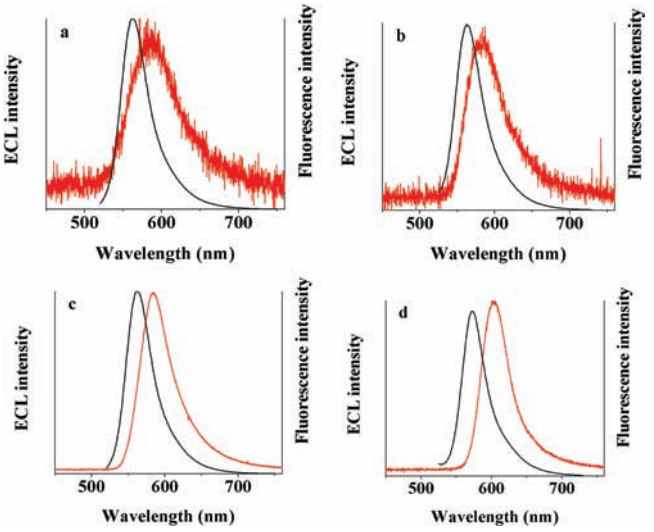

Figure 9. Electrogenerated (red) and fluorescence spectra (black) for the investigated dimers. Annihilation spectrum for 0.14 mM **dimer 1** (a) and 0.2 mM **dimer 2** (b). (c,d) Spectra generated in the presence of 5 mM of benzoyl peroxide. Solvent, DCM; supporting electrolyte, 0.1 M $TBAPF_6$; platinum electrode area, 0.0314 cm^2.

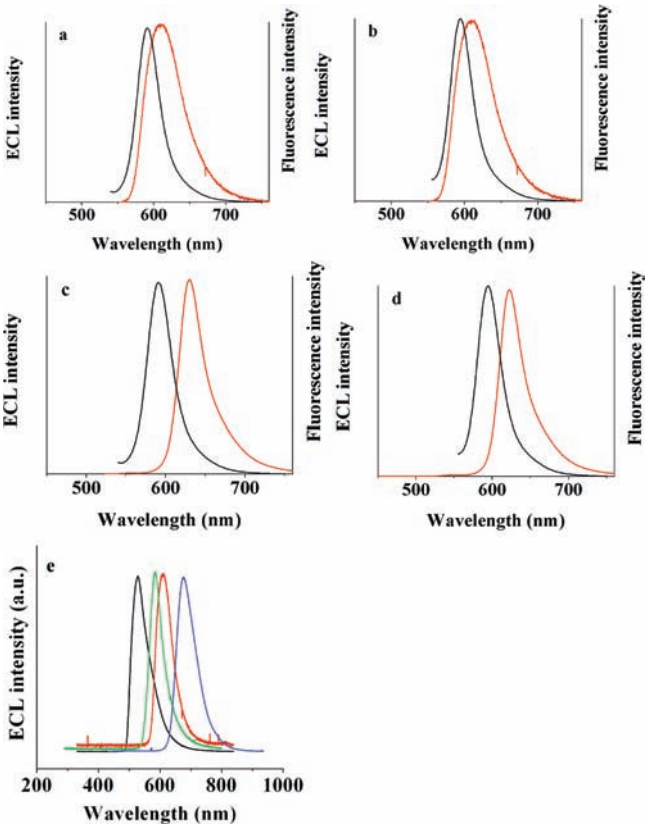

Figure 10. Electrogenerated spectra of the corresponding trimers. Annihilation spectrum for 0.1 mM **trimer 1** (a) and 0.24 mM **trimer 2** (b). (c,d) Spectra generated in the presence of 5 mM of benzoyl peroxide. (e) Comparison of the ECL spectra for 1.0 mM **monomer 1** (black), 0.14 mM **dimer 1** (green), 0.1 mM **trimer 1** (red), and 0.5 mM **angular dimer** (blue) in the presence of 5 mM benzoyl peroxide. All spectra were normalized to the same height. Solvent, DCM; supporting electrolyte, 0.1 M $TBAPF_6$; platinum electrode area, 0.0314 cm^2.

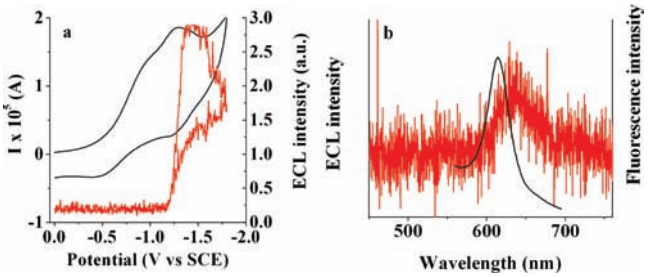

Figure 11. (a) Simultaneous ECL-CV measurement for 0.1 mM **polymer** in the presence of 1 mM benzoyl peroxide at a scan rate of 1 V/s. (b) ECL spectra generated in the presence of 5 mM benzoyl peroxide. Solvent, CH_2Cl_2; supporting electrolyte, 0.2 M $TBAPF_6$; electrode area, 0.12 cm^2.

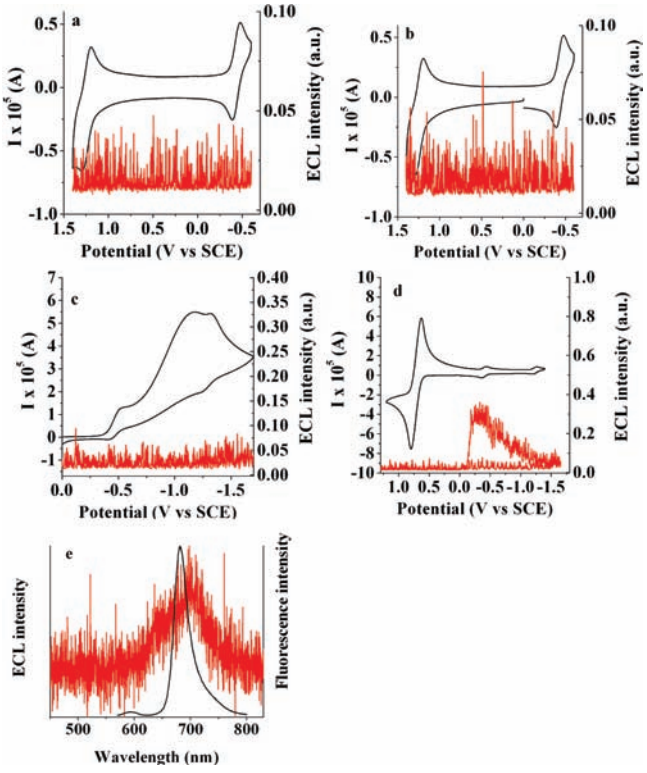

Figure 12. Simultaneous ECL-CV cyclic voltammograms of the 0.5 mM of the **aza-BODIPY monomer** during scans into the (a) negative and (b) positive direction at a scan rate of 1 V/s; (c) in the presence of 3.0 mM benzoyl peroxide; (d) in the presence of 3.0 mM 10-MP. (e) ECL spectra for 0.5 mM (red) and fluorescence spectra (black) for 2 mM **aza-BODIPY monomer** in the presence of 5.0 mM 10-MP. ECL spectrum was generated from 80 mV of the peaks of the reduction of **aza-BODIPY monomer** and oxidation of 10-MP. Solvent, CH_2Cl_2; supporting electrolyte, 0.1 M $TBAPF_6$; electrode area, 0.0314 cm^2.

wavelengths for the dimers and trimers is blue-shifted compared with **angular dimer** in agreement with the fluorescence and electrochemical results (Figure 10e). The mesityl- substituted dyes showed slightly red-shifted ECL compared with the methyl-substituted dyes in agreement with the fluorescence. The energies of annihilation, ΔH_{ann} are close to the E_s values as for all of the BODIPY dyes suggesting direct singlet population or triplet formation followed by triplet−triplet annihilation (the ST route)

dx.doi.org/10.1021/ja2010219 |*J. Am. Chem. Soc.* 2011, 133, 8633–8645

is possible.[21,22,25,28] The **polymer** produced detectable ECL with co-reactant, but not by annihilation ECL (Figure 11).

ECL studies of the **aza-BODIPY monomer** and **aza-BODIPY dimer** did not show substantial ECL by annihilation or by using benzoyl peroxide as a co-reactant (Figure 12). This can be attributed to two factors: one of them is a decrease in the photoluminescence quantum efficiency with a shift of the reduction potential to the positive direction compared with the C^8 dye and the other one is instability on oxidation. The first factor is probably more important, as there was substantial annihilation ECL signal for C^8 BODIPY. A small ECL signal can be produced by a mixed system, with 10-methylphenothiazine (10-MP) as the radical cation precursor (Figure 12c,d).[71−73] In this case the ECL mechanism can be presented as

$$\text{aza-BODIPY} + e^- \rightarrow \text{aza-BODIPY}^{\cdot -} \quad (15)$$

$$\text{10-MP} - e^- \rightarrow \text{10-MP}^{\cdot +} \quad (16)$$

$$\text{aza-BODIPY}^{\cdot -} + \text{10-MP}^{\cdot +} \rightarrow {}^3\text{aza-BODIPY} + \text{10-MP} \quad (17)$$

$${}^3\text{aza-BODIPY} + {}^3\text{aza-BODIPY} \rightarrow {}^1\text{aza-BODIPY}^* + \text{aza-BODIPY} \quad (18)$$

$${}^1\text{aza-BODIPY}^* \rightarrow \text{aza-BODIPY} + h\nu \quad (19)$$

The presence of the ECL signal in this case can be explained by higher stability of the 10-MP radical cation. The **aza-BODIPY dimer** does not show any substantial ECL signal under any conditions, which is consistent with its low fluorescence intensity and also the relatively positive potentials for reduction.

CONCLUSIONS

Monomeric, dimeric, trimeric and polymeric structures of C^8 BODIPY and monomeric and dimeric aza-BODIPY were synthesized. Dimers and trimers were synthesized through oxidative coupling between the 2/6-position with $FeCl_3$. Electrochemical studies show correlation of the number of active units with the amount of electrochemical peaks from monomer to oligomer. Cyclic voltammetry shows that the interaction, and hence the potential splitting between consecutive peaks increases in the order monomer < dimer < trimer, with a larger separation between two consecutive peaks for the oxidation process compared with the reduction one. The same phenomenon is seen for the **aza-BODIPY monomer** and dimer. ECL spectra were generated for all C^8 systems, which show a small increase in the annihilation efficiency from monomer to dimer to trimer. A substantial increase in the ECL efficiency occurred when benzoyl peroxide was used as a co-reactant. **Polymer** and **aza-BODIPY monomer** show very small or no ECL due to the reactivity of the radical ions. No ECL is found for the **aza-BODIPY dimer**.

These electrochemical and spectroscopic characterizations of small oligomers of BODIPYs should help in development of new polymeric dyes for new applications.

ASSOCIATED CONTENT

Supporting Information. Additional figures and experimental information. This material is available free of charge via the Internet at http://pubs.acs.org.

AUTHOR INFORMATION

Corresponding Author
ajbard@mail.utexas.edu

ACKNOWLEDGMENT

We thank the Center for Electrochemistry, Roche, Inc., the Robert A. Welch Foundation (F-0021), and Deutsche Forschungsgemeinschaft for support of this research and Andy Tennyson for help in THF purification.

REFERENCES

(1) Loudet, A.; Burgess, K. *Chem. Rev.* **2007**, *107*, 4891–4932.
(2) Sathyamoorthi, G.; Boyer, J. H.; Allik, T. H.; Chandra, S. *Heteroat. Chem.* **1994**, *5*, 403–407.
(3) Pavlopoulos, T. G.; Shah, M.; Boyer, J. H. *Appl. Opt.* **1988**, *27*, 4998–4999.
(4) Pavlopoulos, T. G.; Shah, M.; Boyer, J. H. *Opt. Commun.* **1989**, *70*, 425–427.
(5) Wang, D.; Miyamoto, R.; Shiraishi, Y.; Hirai, T. *Langmuir* **2009**, *25*, 13176–13182.
(6) Kennedy, D. P.; Kormos, C. M.; Burdette, S. *J. Am. Chem. Soc.* **2009**, *131*, 8578–8586.
(7) Rosenthal, J.; Lippard, S. J. *J. Am. Chem. Soc.* **2009**, *132*, 5536–5537.
(8) Lee, Y. C.; Hupp, J. T. *Langmuir* **2010**, *26*, 3760–3765.
(9) Godoy, J.; Vives, G.; Tour, J. M. *Org. Lett.* **2010**, *12*, 1464–1467.
(10) Nierth, A.; Kobitski, A. Y.; Nienhaus, G. U.; Jäschke, A. *J. Am. Chem. Soc.* **2010**, *132*, 2646–2654.
(11) Frein, S.; Camerel, F.; Ziessel, R.; Barbera, J.; Deschenaux, R. *Chem. Mater.* **2009**, *21*, 3950–3959.
(12) Bañuelos, J.; Arbeloa, F. L.; Arbeloa, T.; Sallares, S.; Amat-Guerri, F.; Liras, M.; Arbeloa, I. L. *J. Phys. Chem. A* **2008**, *112*, 10816–10822.
(13) Yogo, T.; Urano, Y.; Ishitsuka, Y.; Maniwa, F.; Nagano, T. *J. Am. Chem. Soc.* **2005**, *127*, 12162–12163.
(14) Meng, G.; Velayudham, S.; Smith, A.; Luck, R.; Liu, H. *Macromolecules* **2009**, *42*, 1995–2001.
(15) Thivierge, C.; Bandichhor, R.; Burgess, K. *Org. Lett.* **2007**, *9*, 2135–2138.
(16) Kamiya, M.; Johnsson, K. *Anal. Chem.* **2010**, *82*, 6472–6479.
(17) Ojida, A.; Sakamoto, T.; Inoue, M.; Fujishima, S.; Lippens, G.; Hamachi, I. *J. Am. Chem. Soc.* **2009**, *131*, 6543–6548.
(18) Zhang, X.; Xiao, Y.; Qian, X. *Angew. Chem., Int. Ed.* **2008**, *47*, 8025–8029.
(19) Cheng, T.; Xu, Y.; Zhang, S.; Zhu, W.; Qian, X.; Duan, L. *J. Am. Chem. Soc.* **2008**, *130*, 16160–16161.
(20) Huh, J. O.; Do, Y.; Lee, M. H. *Organometallics* **2008**, *27*, 1022–1025.
(21) Lai, R. Y.; Bard, A. J. *J. Phys. Chem. B* **2003**, *107*, 5036–5042.
(22) Sartin, M. A.; Camerel, F.; Ziessel, R.; Bard, A. J. *J. Phys. Chem. C.* **2008**, *112*, 10833–10841.
(23) Trieflinger, C.; Röhr, H.; Rurack, K.; Daub, J. *Angew. Chem., Int. Ed.* **2005**, *44*, 6943–6947.
(24) Benniston, A. C.; Copley, G.; Harriman, A.; Howgego, D.; Harrington, R. W.; Clegg, W. *J. Org. Chem.* **2010**, *75*, 2018–2027.
(25) Nepomnyashchii, A. B.; Cho, S.; Rossky, P. J.; Bard, A. J. *J. Am. Chem. Soc.* **2010**, *132*, 17550–17559.
(26) Rachford, A. A.; Ziessel, R.; Bura, T.; Retailleau, P.; Castellano, F. N. *Inorg. Chem.* **2010**, *49*, 3730–3736.
(27) Dumas-Verdes, C.; Miomandre, F.; Lepicier, E.; Galangau, O.; Vu, T. T.; Clavier, G.; Meallet-Renault, R.; Audebert, P. *Eur. J. Org. Chem.* **2010**, 2525–2535.
(28) Nepomnyashchii, A. B; Bröring, M.; Ahrens, J.; Krüger, R.; Bard, A. J. *J. Phys. Chem. C* **2010**, *114*, 14453–14460.
(29) Flanagan, J. B.; Margel, S.; Bard, A. J.; Anson, F. C. *J. Am. Chem. Soc.* **1978**, *100*, 4248–4253.

(30) Astruc, D.; Ornelas, C.; Ruiz, J. *Chem.—Eur. J.* **2009**, *15*, 8936–8944.
(31) Wang, A.; Ornelas, C.; Astruc, D.; Hapiot, P. *J. Am. Chem. Soc.* **2009**, *131*, 6652–6653.
(32) Ornelas, C.; Ruiz, J.; Belin, C.; Astruc, D. *J. Am. Chem. Soc.* **2009**, *131*, 590–601.
(33) Amatore, C.; Bouret, Y.; Maisonhaute, E.; Goldsmith, J. I.; Abruña, H. D. *Chem.—Eur. J.* **2001**, *7*, 2206–2226.
(34) Guay, J.; Kasai, P.; Diaz, A.; Wu, R.; Tour, J. M.; Dao, L. H. *Chem. Mater.* **1992**, *4*, 1097–1105.
(35) Mitshke, U.; Bäuerle, P. *J. Chem. Soc., Perkin Trans.* **2001**, *1*, 740–753.
(36) Müller, U.; Baumgarten, M. *J. Am. Chem. Soc.* **1995**, *117*, 5840–5850.
(37) Itaya, K.; Bard, A. J.; Szwarc, M. *Z. Phys. Chem. NF* **1978**, *112*, 1–9.
(38) Grabner, G.; Rechthaler, K.; Köhler, G. *J. Phys. Chem. A* **1998**, *102*, 689–696.
(39) Baumgarten, M.; Gheral, L.; Friedrich, J.; Jurczok, M.; Rettig, W. *J. Phys. Chem. A* **2000**, *104*, 1130–1140.
(40) Hill, M. G.; Penneau, J.-F.; Zinger, B.; Mann, K.; Miller, L. L. *Chem. Mater.* **1992**, *4*, 1106–1113.
(41) Allik, T. H.; Hermes, R. E.; Sathyamoorthi, G.; Boyer, J. H. *Proc. SPIE-Int. Soc. Opt. Eng.* **1994**, *2115*, 240–248.
(42) Gorman, A.; Killoran, J.; O'Shea, C.; Kenna, T.; Gallagher, W. M.; O'Shea, D. F. *J. Am. Chem. Soc.* **2004**, *126*, 10619–10631.
(43) McDonnell, S. O.; O'Shea, D. F. *Org. Lett.* **2006**, *8*, 3493–3496.
(44) Bouit, P. A.; Kamada, K.; Feneyrou, P.; Berginc, G.; Toupet, L.; Maury, O.; Andraud, C. *Adv. Mater.* **2009**, *21*, 1151–1154.
(45) Loudet, A.; Bandichhor, R.; Wu, L.; Burgess, K. *Tetrahedron* **2008**, *64*, 3642–3654.
(46) Ulrich, G.; Ziessel, R.; Harriman, A. *Angew. Chem., Int. Ed.* **2008**, *47*, 1184–1201.
(47) Sasaki, E.; Kojima, H.; Nishimatsu, H.; Urano, Y.; Kikuchi, K.; Hirata, Y.; Nagano, T. *J. Am. Chem. Soc.* **2005**, *127*, 3684–3685.
(48) Lee, H.; Berezin, M. Y.; Guo, K.; Kao, J.; Achilefu, S. *Org. Lett.* **2009**, *11*, 29–32.
(49) Murtagh, J.; Frimannsson, D. O.; O'Shea, D. F. *Org. Lett.* **2009**, *11*, 5386–5389.
(50) Rihn, S.; Erdem, M.; De Nicola, A.; Retailleau, P.; Ziessel, R. *Org. Lett.* **2011**, *13*, 1916–1919.
(51) Shah, M.; Thangaraj, K.; Soong, M.-L.; Wolford, L. T.; Boyer, J. H.; Politzer, I. R.; Pavlopoulos, T. G. *Heteroat. Chem.* **1990**, *1*, 389–399.
(52) Sathyamoorthi, G.; Soong, M.-L.; Ross, T. W.; Boyer, J. H. *Heteroat. Chem.* **1993**, *4*, 603–608.
(53) Sahami, S.; Weaver, M. *J. Electroanal. Chem.* **1981**, *122*, 155–170.
(54) Rudolph, M. *J. Electroanal. Chem.* **1991**, *314*, 13–22.
(55) Rudolph, M. *J. Electroanal. Chem.* **1992**, *338*, 85–98.
(56) Mocak, J.; Feldberg, S. W. *J. Electroanal. Chem.* **1997**, *378*, 31–37.
(57) Feldberg, S. W.; Goldstein, C. I.; Rudolph, M. *J. Electroanal. Chem.* **1996**, *413*, 25–36.
(58) Negishi, E., Ed. *Handbook of Organopalladium Chemistry for Organic Synthesis*; John Wiley & Sons: New York, 2002.
(59) Camerel, F.; Bonardi, L.; Schmutz, M.; Ziessel, R. *J. Am. Chem. Soc.* **2006**, *128*, 4548–4549.
(60) Bröring, M.; Krüger, R.; Link, S.; Kleeberg, C.; Köhler, S.; Xie, X.; Ventura, B.; Flamigni, L. *Chem.—Eur. J.* **2008**, *14*, 2976–2983.
(61) Ventura, B.; Marconi, G.; Bröring, M.; Krüger, R.; Flamigni, L. *New J. Chem.* **2009**, *33*, 428–438.
(62) Kasha, M.; Rawls, R.; El-Bayoumi, M. A. *Pure Appl. Chem.* **1965**, *11*, 371–392.
(63) Prieto, J. B.; Arbeloa, F. L.; Martinez, V. M.; Lopez, T. A.; Arbeloa, I. L. *Phys. Chem. Chem. Phys.* **2004**, *6*, 4247–4253.
(64) Omer, K. M.; Kanibolotsky, A. L.; Skabara, P. J.; Perepichka, I. F.; Bard, A. J. *J. Phys. Chem. B* **2007**, *111*, 6612–6619.
(65) Bard, A. J. *Pure Appl. Chem.* **1971**, *25*, 379–394.
(66) Meerholz, K.; Heinze, J. *J. Am. Chem. Soc.* **1989**, *111*, 2325–2326.
(67) Müllen, K. *Chem. Rev.* **1984**, *84*, 603–646.
(68) Chandross, E. A.; Sonntag, F. I. *J. Am. Chem. Soc.* **1966**, *88*, 1089–1096.
(69) Akins, D. L.; Birke, R. L. *Chem. Phys. Lett.* **1974**, *29*, 428–435.
(70) Santa-Cruz, T. D.; Akins, D. L.; Birke, R. L. *J. Am. Chem. Soc.* **1976**, *98*, 1677–1682.
(71) Freed, D. J.; Faulkner, L. R. *J. Am. Chem. Soc.* **1971**, *93*, 3565–3568.
(72) Keszthelyi, C. P.; Tachikawa, H.; Bard, A. J. *J. Am. Chem. Soc.* **1972**, *94*, 1522–1527.
(73) Slaterbeck, A. F.; Meehan, T. D.; Gross, E. M.; Wightman, R. M. *J. Phys. Chem. B* **2002**, *106*, 6088–6095.